Macromolecules
ARTICLE

Macromolecules **2010**, *43*, 5033–5042 **5033**
DOI: 10.1021/ma902836n

Patterning of a Surface Immobilized ATRP Initiator with an Inkjet Printer

Sebastian G. J. Emmerling,[†,‡] Laura B. N. Langer,[†] Sascha A. Pihan,[†] Philipp Lellig,[†,‡] and Jochen S. Gutmann*[,‡]

[†]*Max Planck Institute for Polymer Research, Ackermannweg 10, D-55128 Mainz, Germany, and* [‡]*Institute of Physical Chemistry, Johannes Gutenberg University Mainz, Jakob-Welder-Weg 11, D-55128 Mainz, Germany*

Received December 23, 2009; Revised Manuscript Received March 28, 2010

ABSTRACT: A new technique for patterning polymer brushes on the micrometer scale has been developed in which an inkjet printer was used to deposit droplets of acid on a surface-immobilized initiator for atom transfer radical polymerization (ATRP). The acid cleaved an ester bond in the ATRP initiator in a saponification reaction. As a result, the ATRP initiator was rendered inactive. To control the degree of defunctionalization, a new initiator containing a weak ester bond was derived from a tertiary alcohol. Comparison to an established ATRP initiator, derived from a primary alcohol, showed that the novel initiator was defunctionalized with a higher efficiency. Control of the reaction time allowed to partially defunctionalize the initiator molecules, leading to control of grafting densities within the written patterns.

Introduction

Fabrication of polymer brush patterns over large areas remains a demanding task, despite recent achievements using photolithography[1] and microcontact printing (μCP).[2,3] A combination of templating techniques and polymer brush synthesis techniques to amplify the patterns is essential.[4] In this publication we will introduce a versatile fabrication method to pattern polymer brushes on the micrometer scale. This process focuses on flexibility regarding choice of substrates, control of brush length, and the possibility for automation. Among the existing techniques, μ-CP would be the most suitable, but its automation is not easily achieved. We resorted to inkjet printing, circumventing the use of masters and stamps, instead directly writing our patterns on the substrate. Additionally, the new technique enabled us to create gradients in grafting densities over large areas.

Access to brushes with high grafting density has become available through surface-initiated polymerization (SIP) techniques,[5] also commonly referred to as "grafting from".[6] Controlled free-radical polymerization techniques, such as nitroxide-mediated radical polymerization[7] (NMP), reversible addition−fragmentation chain transfer polymerization,[8,9] (RAFT) and atom transfer radical polymerization[10,11] (ATRP), are frequently employed. All these techniques have a wide range of polymerizable monomers in common. Even monomers carrying functional groups can be polymerized. Another advantage is the possibility of creating block copolymer brushes[12] by the reactivation of dormant chain ends in the presence of an additional monomer. Further, transformation of the functional end groups is feasible. ATRP is set apart from the other techniques in a number of ways. Not only has surface-initiated ATRP (SI-ATRP) been reported on a broad range of substrates, viz., silicon wafers,[13,14] silica (nano)particles,[15,16] flexible polymer films,[2] and others.[17,18] In addition this technique can be performed under mild conditions at low temperatures,[19] and most of the reagents are commercially available. A common approach is the covalent self-assembly of initiator species on a substrate.

*Corresponding author: e-mail gutmann@mpip-mainz.mpg.de; Ph +49-6131-379117; Fax +49-6131-379100.

Soon after the initial interest in polymer brushes, researchers no longer solely focused on covering entire surfaces with polymer brushes. In 1995 Rühe and co-workers published three different methods for achieving lateral patterning of a polymer coating.[20] Rühe's group recognized from the beginning the potential application for these patterned surfaces that control the adhesion of biological cells to solid substrates.[21] Research is still focusing on biological applications in this area.[22] Photolithography has also been investigated for patterning by the Hawker group.[23] In addition to deep and near-UV irradiation, electron beams[1] have been deployed. Both these approaches require the use of shadowing masks if larger areas are to be patterned. This is a drawback to keeping production costs low. The major advantage of using shadowing masks, however, is the resolution in the nanometer range. Alongside the development of photolithography and e-beam (chemical) lithography (EBL), various other lithography techniques for pattern formation have been developed. This is highlighted in a recent review.[24] Under the term scanning probe lithography (SPL) are grouped techniques like nanoshaving[25] and dip-pen nanolithography.[26] As the name suggests, these techniques rely on the use of atomic force microscopes (AFM) to manipulate SAMs. The popularity of SPL-techniques stem from the fact that they are technologically simpler compared to EBL, while maintaining a resolution close to that of EBL. When it comes to patterning of large areas, SPL techniques are at disadvantage. This could potentially be mitigated by the use of cantilever arrays. Soft lithography has attracted by far the most interest among all techniques available for creating laterally structured brushes. Developed in the 1990s by Whitesides and co-workers,[27,28] soft lithography using polymer stamps to deliver patterns was utilized to create initiator functionalized micropatterns for SIP. This technique is also known as microcontact printing (μCP). A thiol containing an initiator moiety for ring-opening polymerization (ROP)[29] or ATRP[30−33] is delivered with a stamp onto a gold-covered substrate. Then the uncovered regions are backfilled with a nonfunctional thiol or vice versa. Huck and co-workers[34] developed this approach further by repeating cycles of printing initiator thiols, ATRP thereof, and passivating the "living" chain ends by nucleophilic substitution

Published on Web 05/14/2010

Scheme 1. Structures of 4-(Chlorodimethylsilyl)-2-methylbutan-2-yl 2-bromo-2-methylpropanoate (1) and 3-(Chlorodimethylsilyl)propyl 2-bromo-2-methylpropanoate (2)[a]

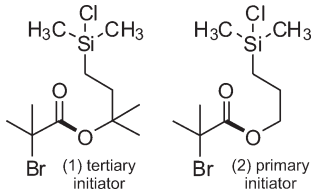

[a] SI-ATRP initiators deployed for "grafting-from" of MMA on silicon wafers in this study. The ester bond (bold) in both initiators can be cleaved under acidic conditions.

with NaN_3. After performing three repeat cycles and one backfilling step, they obtained laterally distinctive multicomponent polymer brushes. Inherent difficulties of this approach include the preparation and handling of the gold films, a potential edge roughness[35] of the written patterns, and delamination. Working with oxidized silicon layers can circumvent some of these problems. First of all, the Si−O bond dissociation energy of 96−133 kcal/mol is higher than the Au−S bond energy at 30−40 kcal/mol. Hence, by using silane/silica chemistry, the layers stay anchored even above 70 °C where Au−S bonds become unstable.[36] However, few publications on the subject of μCP and SIP on SiO_2 can be found.[37−39] We attribute this to difficulties in the reproducible formation of organosilane monolayer patterns by μCP for SIP. Indeed, all cited procedures require several steps to create patterns of "initiator" silanes instead of direct deposition of "initiator" silanes.

This publication describes a route to circumvent the above-stated problems with μCP and SIP on silicon surfaces by a direct and easy one-step approach. We do not create patterns by μCP, but by the use of a computer-assisted drop-on-demand inkjet system and amplify these by ATRP of MMA. The major advantage offered by inkjet printing is the ability to write patterns directly onto substrates, eliminating the use of masks or masters, combined with a resolution of hundreds of nanometers.[40−45]

Furthermore, the computer control of inkjet printers enables fully automated and high throughput manufacturing of patterned materials. This prompted Sankhe et al.[46] to combine inkjet printing with ATRP to produce patterned polymer surfaces. Their work, however, is limited to gold/thiol chemistry, as they print a bromine-containing thiol for ATRP and backfill with a non-ATRP active thiol (or vice versa). Controlling the reaction parameters of the backfilling step proved to be critical, since the printed thiol monolayer was otherwise replaced by the backfilling thiol.

In this article we report on a one-step approach to create patterns with a focus on silicon/silane chemistry, since silane layers on silicon are thermally more stable compared to thiol layers on gold. Nevertheless, our approach is also applicable to gold/thiol chemistry. Contrary to Sankhe et al., we covered the entire surface of the wafer with a silane monolayer of an ATRP initiator and used the inkjet printer to chemically alter this monolayer. The ATRP initiator contains a hydrolytically labile bromoester functionality (see Scheme 1, bold bond). We printed acids to cleave the molecule at this point and pattern the initiator SAM in this way. After cleavage, the surface contains fewer bromo functionalities in the contact areas that participate in ATRP. The thickness of PMMA brushes that grew in the contact areas was thus reduced. The observed changes in film thickness in the contact areas are related to changes in grafting density as an effect of the cleavage of a fraction of ATRP initiators. The results obtained with a common ATRP initiator[47] (depicted in Scheme 1, structure **2**) led us to the synthesis of a more labile ATRP initiator (depicted in Scheme 1, structure **1**). The novel initiator also contains a bromoester functionality but is derived from a tertiary alcohol. In this initiator the ester bond was much more labile and easier to cleave, allowing us to suppress brush growth completely.

Two aspects of the saponification reaction of the SI-ATRP initiator are discussed in this study. First, we investigated the usefulness of hydrochloric acid or sulfuric acid in saponification of the initiator monolayer and its concentration dependence. To obtain results independent of initial SAM preparation, we used the inkjet printer to screen these parameters on one substrate. Second, we investigated the time dependence of the saponification reaction by controlling the contact time between acid and initiator. In this way we achieved a gradual variation of grafting density from the brush regime to the mushroom regime[48] over the area of a silicon piece the size of 2.3 × 3 cm using a dip-coater.

Experimental Section

Materials. Allymagnesium bromide (1.0 M in diethyl ether, Aldrich), 2-bromoisobutyryl bromide (97%, Alfa), pyridine (99%, Aldrich), chlorodimethylsilane (95%, Fluka), dihydrogen hexachloroplatinate(IV) hexahydrate (99.9% metals basis, Alfa), ethyl α-bromoisobutyrate (97%, Fluka), toluene (anhydrous 99,8%, Aldrich), sulfuric acid (purum p.a. 95−97%, Fluka), and hydrochloric acid (37%, Aldrich) were used as received.

Copper bromide (98%, Aldrich) was purified by boiling it for a short time in a mixture of 50:50 v/v Millipore water/glacial acetic acid and thereafter filtered off. This was followed by rinsing the precipitate with water, ethanol, and diethyl ether, and finally it was dried under reduced pressure for 24 h.[49]

Methyl methacrylate (MMA) (99%, Acros) was purified by passing it through an alumina column, distilled under reduced pressure from CaH_2, and stored under argon at −20 °C.

N,N,N′,N′,N″-Pentamethyldiethylenetriamine (PMDETA) (99%, Aldrich) was purified by distillation under reduced pressure and triethylamine by distillation from CaH_2 in an argon atmosphere.

Instrumentation. A Nano-Plotter NP 2.0 (GeSIM GmbH, Germany) was used to dispense droplets of acid onto the silicon surface covered with a monolayer of ATRP initiator. The plotter consists of a mobile pipet dispenser and a work plate that can be cooled. During time-dependent saponification experiments the temperature was set to 10 °C. All other printing experiments were conducted at room temperature (20 °C). The dispenser is equipped with a piezo-driven microdosage head that works in a noncontact regime. Its positioning can be fully controlled along the plane parallel to the substrate with a speed of 50 cm/s.

An imaging ellipsometer (EP3 Imaging Spectroscopic Ellipsometer, Nanofilm, Goettingen, Germany) was used to determine the thickness of the polymer brush layer. It was operated at a wavelength $\lambda = 532$ nm, an angle of incidence $\alpha_i = 60°$, and a field of view of 0.39 × 0.3 mm (horizontal × vertical). The calculation of PMMA thickness was conducted using a multilayer model (Air, PMMA, initiator monolayer, SiO_2, amorphous Si).[50] The SiO_2 ($n_{SiO_2} = 1.46$) and initiator layer ($n_{Initiator} = 1.4603$) were treated as one layer due to the small difference in refractive indices and set to $n = 1.46$. Furthermore, for the refractive index of the dry PMMA brush film $n_{PMMA} = 1.49$ was used. With the above stated values, the error for reported layer thickness was calculated as ±1 nm.

Analysis of the bulk PMMA was carried out at 20 °C with a GPC setup consisting of the following components: Waters 515 HPLC pump, Waters WISP717 autosampler, three Polymers Standard Service columns (SDV) in series (dimension: 300 × 8 mm, porosity: 500, 10^5, and 10^6 Å, respectively), filled with poly(styrene/divinylbenzene), and an ERC refractive index detector along with a UV-Soma detector. Tetrahydrofuran, at a flow rate of 1 mL min^{-1}, was used as an eluent. Calibration was done applying low-polydispersity poly(methyl methacrylate) standards.

Scheme 2. Synthesis of the Tertiary SI-ATRP Initiator

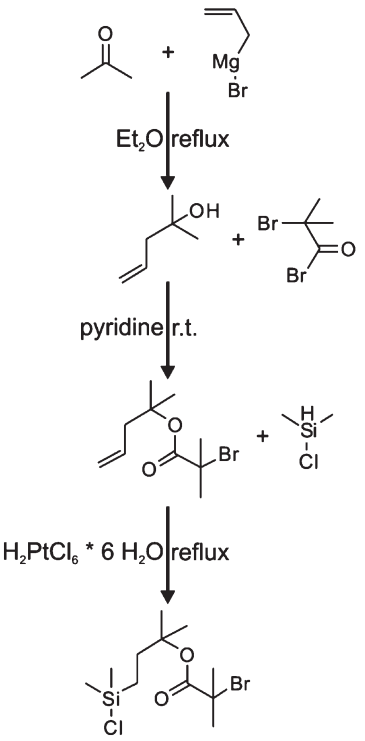

All ^{1}H NMR spectra were recorded with a Bruker DPX250, operating at 250 MHz in deuterated chloroform, and the spectra were calibrated on this solvent.

Contact angle measurements were conducted using a Kruess DSA10-MK2 tensiometer. Static contact angles were obtained in air at room temperature with Millipore water as solution.

AFM under ambient conditions was carried out with a Dimension 3100 setup connected to a NanoScopeV controller (Dimension 3100, Veeco). Silicon cantilevers (OMCL-AC 160 TS-W2, Olympus, Japan) with a tip radius of ~10 nm were used in the tapping mode with a resonance-frequency near 300 kHz. Images were recorded in retrace line direction.

Synthesis of SI-ATRP Initiator Derived from the Tertiary Alcohol 2-Methyl-4-penten-2-ol (Depicted in Scheme 2). *First Step: Synthesis of 2-Methyl-4-penten-2-ol Using the Barbier−Grignard Reaction*[51]. The reaction was carried out in a two-neck round-bottom flask equipped with a pressure-equalizing dropping funnel, a condenser, and a magnetic stir bar. Allylmagnesium bromide (in Et_2O; 200 mL, 0.2 mol) was placed in the flask in a protective argon atmosphere and cooled using an ice bath. Under stirring, acetone (14.7 mL, 0.2 mol) was added dropwise (30 min) to the bromide using a dropping funnel while maintaining the temperature at 0 °C. After the addition was completed, the solution was refluxed for 1 h. While cooling, 70 mL of Milli-Q water was added dropwise (20 min), generating a white solid residue. The temperature was kept around 0 °C, and 60 mL of half-concentrated HCl was added dropwise (5 min). The white residue was dissolved and the pH set to 2. For further work-up the solution was transferred to a separatory funnel. The aqueous phase was separated and washed twice with diethyl ether. These ether extracts were combined with the organic phase, washed with little water, dried ($MgSO_4$), and finally evaporated under reduced pressure to yield the crude alcohol. The final product (12.58 g, 62.8%) was attained by fractional destillation and had a boiling point of 117 °C.

Second Step: Synthesis of 2-Methylpent-4-en-2-yl 2-bromo-2-methylpropanoate Using the Pyridine Method of Einhorn[52]. Pyridine (102 mL, 1.26 mol) and 2-methyl-4-penten-2-ol (12.58 g, 0.126 mol) were placed in a protective argon atmosphere in a two-neck round-bottom flask equipped with a pressure-equalizing dropping funnel, a condenser, and a magnetic stir bar. While cooling the flask with an ice bath, 2-bromoisobutyryl bromide (16 mL, 0.126 mol) was added slowly (25 min), forming a yellow precipitate. After heating in a water bath for 15 min, agitation was continued overnight under ambient conditions. The suspension was poured into ice water, and the pH was lowered from 6 to 2 by slow addition of concentrated HCl. The precipitate was dissolved, leaving a clear yellow solution. For further processing, the solution was transferred to a separatory funnel, and the crude product extracted by washing three times with dichloromethane. This slightly acidic organic phase was neutralized by washing with an aqueous solution of hydrogen carbonate (2×). Residual salt was removed by washing with water, and then the solution was dried over $MgSO_4$. The solvent was removed under reduced pressure, and subsequently vacuum distillation (0.1 mbar) of the yellow oil yielded the ester (23 g, 73.3%) with a boiling point of 80 °C as a colorless liquid. ^{1}H NMR δ (ppm): 5.85−5.71 (m, 1H, =CH−); 5.1−5.03 (m, 2H, $=CH_2$); 2.54−2.51 (d, 2H, $-CH_2-$); 1.85 (s, 6H, $-C(CH_3)_2-Br$); 1.45 (s, 6H, $-C(CH_3)_2-O-$).

Third Step: Synthesis of 4-(Chlorodimethylsilyl)-2-methylbutan-2-yl 2-bromo-2-methylpropanoate by Hydrosilylation Using Hydrogen−Hexachloroplatinate(IV) Hexahydrate[53]. In this step moisture-free conditions are of uttermost importance, since the chlorosilane group in the final product is easily hydrolyzed. To ensure this, the experiment was conducted in a dry argon atmosphere. The reaction was carried out in a Schlenk tube with a condenser and a magnetic stir bar. First a catalytic amount of hydrogen−hexachloroplatinate(IV) hexahydrate was placed in the tube and melted with the use of a blow-drier. The released water was purged by dry argon. Subsequently, 2-methylpent-4-en-2-yl 2-bromo-2-methylpropanoate (8 g, 0.03 mol) as well as chlorodimethylsilane (30 mL, 0.27 mol) was added, forming a white residue. After refluxing overnight, a clear red liquid had formed. By distillation under normal pressure the excess chlorosilane was removed. Finally, vacuum distillation (0.1 mbar) allowed us to obtain the clean product (9.54 g, 96.4%) as a colorless oil (bp 110 °C). Degradation by moisture during storage was prevented by placing the initiator under an argon atmosphere over silica gel in a desiccator. ^{1}H NMR δ (ppm): 1.87 (s, 6H, $-C(CH_3)_2-Br$); 1.53−1.41 (m, 10H, $-O-C(CH_3)_2-CH_2-CH_2-$); 0.85−0.78 (m, 2H, $-Si-CH_2-$); 0.4 (s, 6H, $-Si(CH_3)_2-Cl$).

Synthesis of SI-ATRP Initiator Derived from the Primary Alcohol Prop-2-en-1-ol (Structure 2 in Scheme 1). The initiator 3-(chlorodimethylsilyl)propyl 2-bromo-2-methylpropanoate was synthesized according to Ramakrishnan et al.[54] However, we opted to do the hydrosilylation step following the above described approach for the tertiary initiator with hydrogen−hexachloroplatinate(IV) hexahydrate. Distillation under reduced pressure was carried out to obtain the pure product, which was also stored in an argon atmosphere over silica gel in a desiccator.

Cleaning of Silicon Wafers. Dust was blown off the 2.3 × 3 cm big wafer in a nitrogen stream. Organic impurities were removed by immersing the wafer in dichloromethane and placing it in an ultrasound bath for 10 min followed by base cleaning. The wafer was placed in a mixture of NH_3 (4 mL, 32%), H_2O_2 (4 mL, 35%), and Milli-Q water (50 mL) at 80−85 °C for 20 min. Finally, the wafer was washed twice with Milli-Q water, desiccated in nitrogen current, and used immediately.

Immobilization of ATRP Initiators. Moisture-free conditions and dry chemicals are of importance in this step since both initiators are easily hydrolyzed. The wafer was mounted in a holder; toluene (25 mL), triethylamine (0.2 mL, 1.435 mmol), and one of the initiators (0.2 mL) were added in a dry argon counter flow. After stirring for 20 h, a suspension formed. The formation of the insoluble salt (TEA·HCl) indicated the successful functionalization of the wafer surface. The resulting silanated wafer was washed with Milli-Q water (2×) and then placed in a Soxhlet apparatus with dichloromethane

Scheme 3. Sample Preparation by (a) Printing the Acid with a Commercially Available Inkjet Printer, (b) Washing, (c) Drying the Sample in a Stream of Nitrogen, (d) ATRP of MMA, and (e) Top View of Sample Prepared by Printing Various Concentrations of H_2SO_4

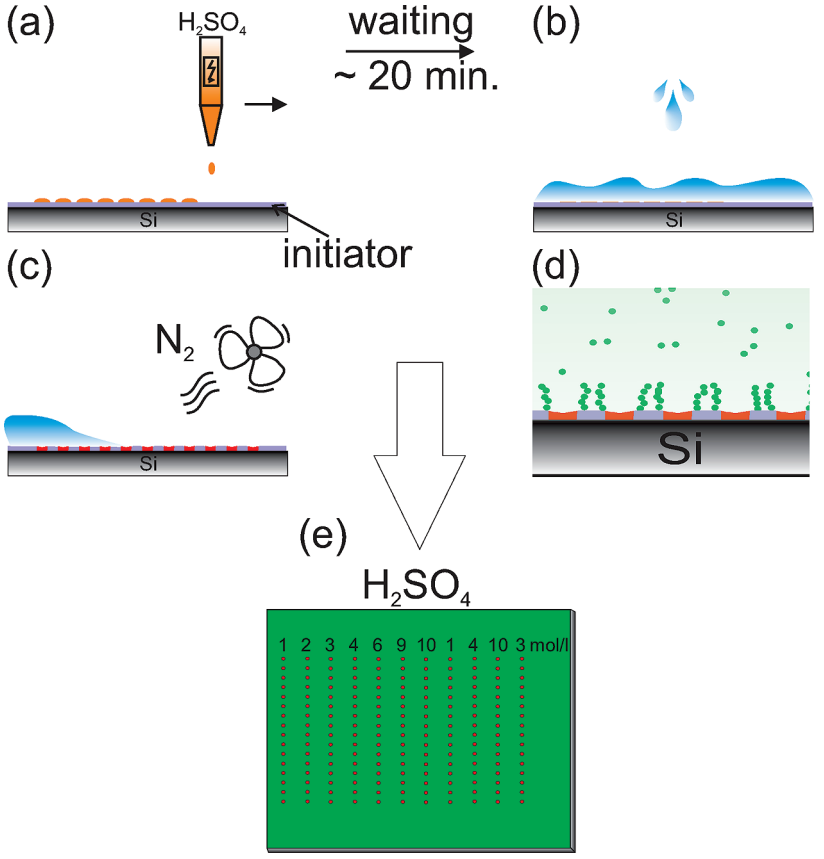

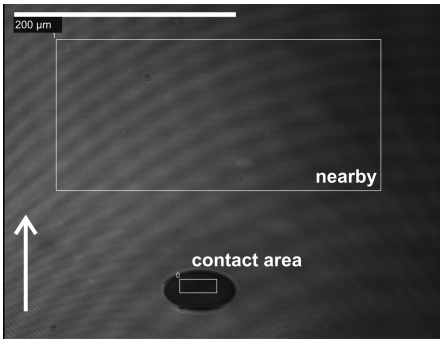

Figure 1. Typical image of data acquisition with the imaging ellipsometer on a sample of patterned PMMA brushes. The white rectangles mark the regions of interest, where the film thickness was acquired. The spherical drop is imaged as elliptical in shape because the image was taken under a viewing angle of 60°. The white arrow indicates viewing direction of the optical system.

overnight to remove any traces of salt and physisorbed initiator molecules.

Application of Acids with the Inkjet Printer. In a typical dispense experiment, a silicon wafer covered with a monolayer of ATRP initiator was mounted onto the working plate of the inkjet printer. The printing nozzle was loaded with either concentrated HCl or one of the different concentrations of H_2SO_4. As depicted in Scheme 3a, single droplets (volume 0.35−0.4 nL) were deposited and arranged in lines. This was completed within seconds. After spreading, the typical droplet size was below 100 μm (see Figure 1). Individual droplets were placed around 300 μm apart from each other. The distance between lines was about 1 mm. The average contact time between the surface and the acid was 20 min, after which the wafer was taken out of the printer and washed with plenty of Milli-Q water (Scheme 3b). This was done to remove the applied acid and the generated bromoisobutyric acid. Subsequently, the wafer was blown dry in a stream of nitrogen (Scheme 3c). In the final step, the PMMA brushes were grown on the surface of the wafer. Reaction details are given in the next paragraph and in Scheme 4. In the areas, where the acid previously had been in contact with the surface, grafting density was lowered. For some concentrations of acid brush growth was completely suppressed. The red areas in Scheme 3d represent these contact areas, and the green dots represent the monomer. Scheme 3e illustrates the top view of the samples prepared for an in-depth study of different concentrations of H_2SO_4. For this purpose two lines of 10, 4, 3, and 1 mol/L H_2SO_4 were printed, along with a line of 9, 6, and 2 mol/L. Data of samples prepared in this fashion are displayed in Figure 4.

Not shown in Scheme 3 are the samples that we prepared in order to compare the effect of concentrated HCl and different concentrations of H_2SO_4 on the ester bond in the initiator molecules. Overall, droplets of concentrated HCl were arranged in three lines. In addition, two lines of 10 and 1 mol/L H_2SO_4 each were printed, along with one line of 6 and 3 mol/L H_2SO_4 and a line of Milli-Q water. The data obtained from these samples are represented in Figure 3.

Application of Acids for Investigation of Time Dependence of Saponification Reaction. Two different approaches were taken to investigate the effect of contact time between H_2SO_4 and both of the initiator SAMs. First of all, we created samples with the inkjet printer that allowed us to compare the effect of the contact time between three different concentrations of H_2SO_4 (1, 0.5, and 0.1 mol/L) on the initiator molecules. To slow the saponification reaction, we cooled the samples to 10 °C. For each concentration we printed a line of droplets every 4 min. 32 min after deposition of the first line, the last line was printed, and

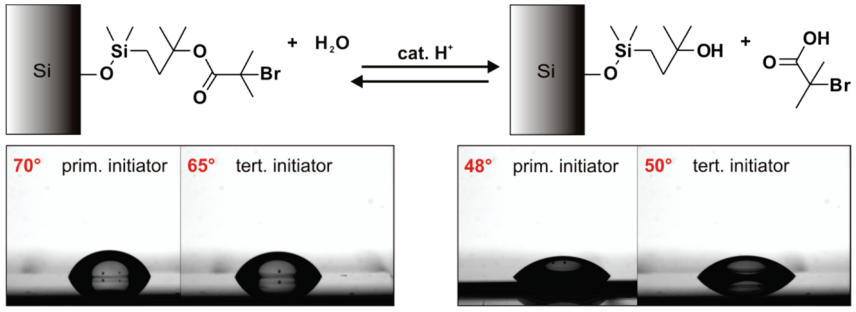

Figure 2. Saponification of surface-immobilized tertiary ATRP initiator with catalytic amount of acid. The error of the contact angles is ±10°.

Scheme 4. Reaction Scheme of SI-ATRP of MMA with Tertiary Initiator Covalently Anchored on a Silicon Surface[a]

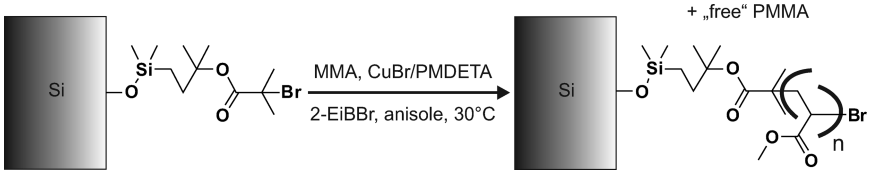

[a] The sacrificial initiator 2-EiBBr generated free polymer.

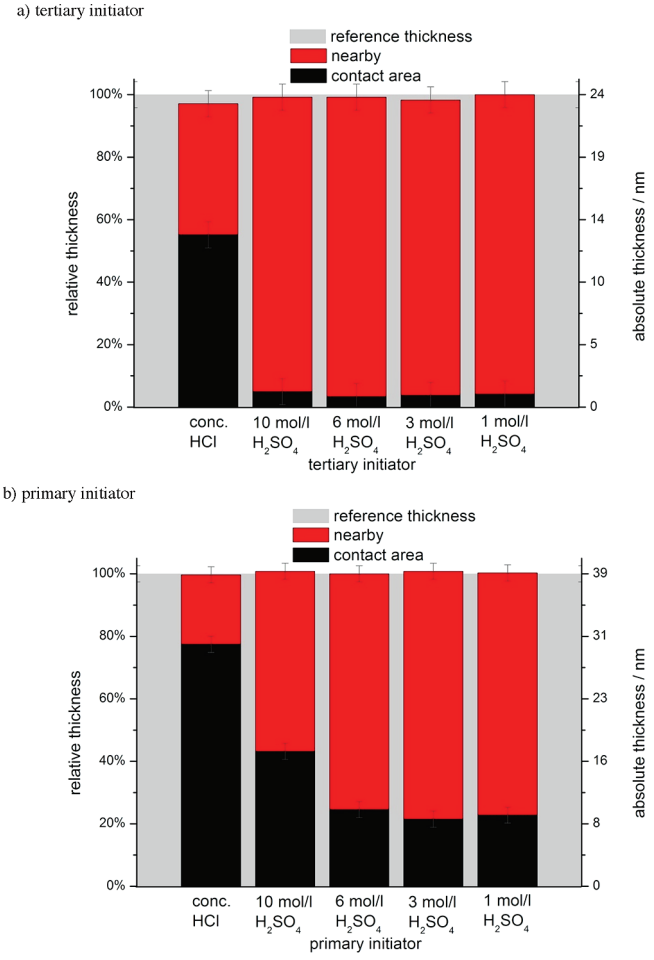

Figure 3. Effect of concentrated HCl and various concentrations of H_2SO_4 on the film thickness of PMMA brushes.

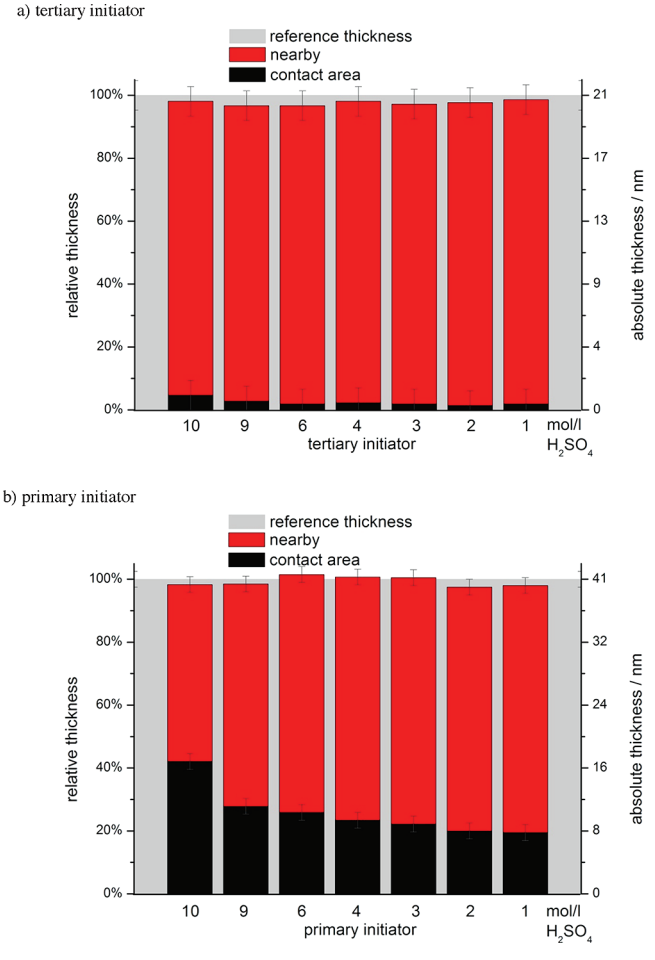

Figure 4. Effect of various concentrations of H_2SO_4 on the film thickness of PMMA grown through SI-ATRP.

after an additional 4 min the wafer was washed and the polymerization started.

In the second approach we utilized a dip-coater. The use of a dip-coater allowed us to create a gradient in grafting density over the area of a whole wafer. Additionally, evaporation plays no role in dip-coating, whereas the small droplets in inkjet printing evaporate rapidly. Two wafers, one coated with the tertiary initiator and one with the primary, were fixed on the dip-coater. These wafers were totally immersed in a solution of

1 mol/L H_2SO_4, except for an area 3 mm in width. Starting after 2 min, the wafers were pulled out of the solution with a speed of 1.5 mm/min.

SI-ATRP of MMA. Surface-initiated ATRP was carried out in a modified Schlenk tube containing the freshly functionalized wafers and a magnetic stir bar. Oxygen-free conditions were ensured by working in an argon atmosphere and by flushing anisole (10 mL) and MMA (10 mL, 0.09 mol) with argon prior to use. Under argon counter flow, CuBr (13.4 mg, 0.09 mmol), anisole, MMA, and PMDETA (19.6 μL, 0.09 mmol) were added to the tube. The active copper complex formed during stirring for 10 min. The slightly green tint of the solution is caused by traces of Cu(II). Subsequent to the addition of the free initiator 2-EiBBr (13.8 μL, 0.09 mmol), the holder was capped with a stopper, and three freeze−pump−thaw cycles were executed. During the course of heating overnight at 30 °C the polymerization proceeded and finally was stopped by exposing the solution to air. The wafers were taken out, washed with dichloromethane, and then extracted with dichloromethane overnight in a Soxhlet apparatus to remove the free polymer. The free polymer generated by the sacrificial initiator was recovered by precipitation into methanol, drying, and subjected to GPC measurement. Molecular weights, grafting densities, and a plot showing the linear dependency of film thickness on molecular weight of the free polymer can be found in the Supporting Information. From the linear dependency of film thickness on molecular weight we concluded that the polymerization proceeds in a controlled way.

If the data of wafers covered with tertiary initiator are compared to the data of wafers covered with primary initiator, the PMMA brushes on both wafers were typically grown in the same solution, ensuring the same molecular weight of polymer molecules.

Data Acquisition and Treatment. PMMA film thicknesses given throughout this publication were acquired with an imaging ellipsometer. This technique allowed us to select certain regions of interest, where we wanted to measure the film thickness. This is sketched in Figure 1. All objects were imaged distorted along the incoming beam (indicated by the white arrow) due to a viewing angle of 60°. A spherical droplet is thus imaged as an ellipse. For information on the calculation of the feature size on the sample surface in vertical direction, see the Supporting Information.

The dark 60 μm wide (horizontal direction) feature was generated by spotting a droplet of acid on the initiator layer prior to polymerization. Little or no polymer grew in this contact area. Therefore, the change in polarization of these areas with thinner films is clearly distinguishable from the polarization of the light induced by the surrounding thicker films.

By contact area (34 × 27 μm/horizontal × vertical size) we refer to the region of interest that was located within one of the patterns. Within the distance of 50−100 μm of the pattern we placed a region of interest labeled nearby (292 × 274 μm/horizontal × vertical size).

A representative value taken as a reference thickness (390 × 300 μm/horizontal × vertical size) was obtained from positions on the wafer that were at least 1 mm away from any dispensed droplet. In these areas the recorded data were not affected by acid. Spraying due to the formation of satellite droplets may occur in inkjet printing as well as spreading of the liquid on the surface.[55] Both these effects could have potentially influenced the nearby film thickness.

On average, we measured eight points on the sample away from patterns to calculate the mean value and plotted it as the reference thickness. The standard deviation was in all cases lower than the error that resulted from the modeling of the ellipsometric angles. Therefore, we chose the error of the modeling (±1 nm) as error bars. We proceeded like this when comparing the data for the two kinds of acids (Figure 3) as well as for the comparison between the different concentrations of H_2SO_4 (Figure 4).

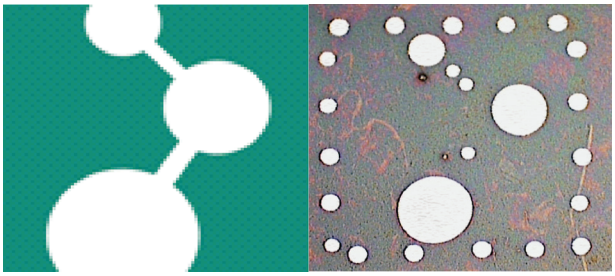

Figure 5. The logo of our institute is shown on the left. On the right side is the pattern after polymerization with PMMA shown. The light regions correspond to no polymer growth, while the regions where polymer was grown appear darker. The image was taken with an optical microscope.

Similarly, mean values for the contact area and nearby are plotted in Figures 3 and 4. On average, four single drops were measured and the mean value was calculated. Once again the margin of error from the modeling of the ellipsometric angles was bigger than the standard deviation from the mean value, so the error of the modeling (±1 nm) was chosen as error bars.

In addition to plotting the data against absolute film thickness, we also chose to plot the data as relative thickness with respect to the reference thickness. Trends in the data are at times more articulated using the relative thickness, since the absolute thickness varies from sample to sample. Several factors, among them the polymerization time and the conversion, are the reason for this. This motivated us to plot the data in Figures 6 and 7 exclusively as relative thickness.

Results and Discussion

Contact Angles: Determination of Surface Properties after Contact with Acid. The basic principle underlying this research is the saponification reaction of surface-immobilized ATRP initiator molecules. Ordinarily, saponification is done on mobile molecules in solution and not on molecules immobilized on a surface. Our first step was therefore to prove that saponification of surface-immobilized molecules is feasible. We performed static contact angle measurements to examine the change in surface energy after the saponification. As depicted in the upper part of Figure 2, quantitative saponification of the tertiary initiator leaves a tertiary alcohol on the surface. The free bromoisobutyric acid can be washed away in the cleaning step. Two wafers were covered with the initiator molecules and contact angles of 70 ± 10° for the primary initiator (compared to 77° from an earlier publication of our group[56]) and 65 ± 10° for the tertiary initiator on the freshly prepared samples measured. The samples were processed further by immersing them halfway into 1 mol/L H_2SO_4 for 40 min to allow the saponification to proceed. A cleaning step—washing with Milli-Q water and extraction with DCM overnight—was performed to remove any residual free bromoisobutyric acid from the surface. No changes in contact angles were observed on the parts of the samples that had not been in contact with the acid. In the contact area we observed a decrease to 48 ± 10° in the case of the primary initiator and 50 ± 10° for the tertiary one. Miyake et al.[57] reported a contact angle for a hydroxyl-terminated SAM of 55°, which is within the error of our observation. This indicates that saponification reactions on surface-immobilized molecules are possible.

Comparison of Effectiveness of Hydrochloric Acid and Sulfuric Acid in Saponification. In general, saponification is an equilibrium reaction. The reaction conditions must be

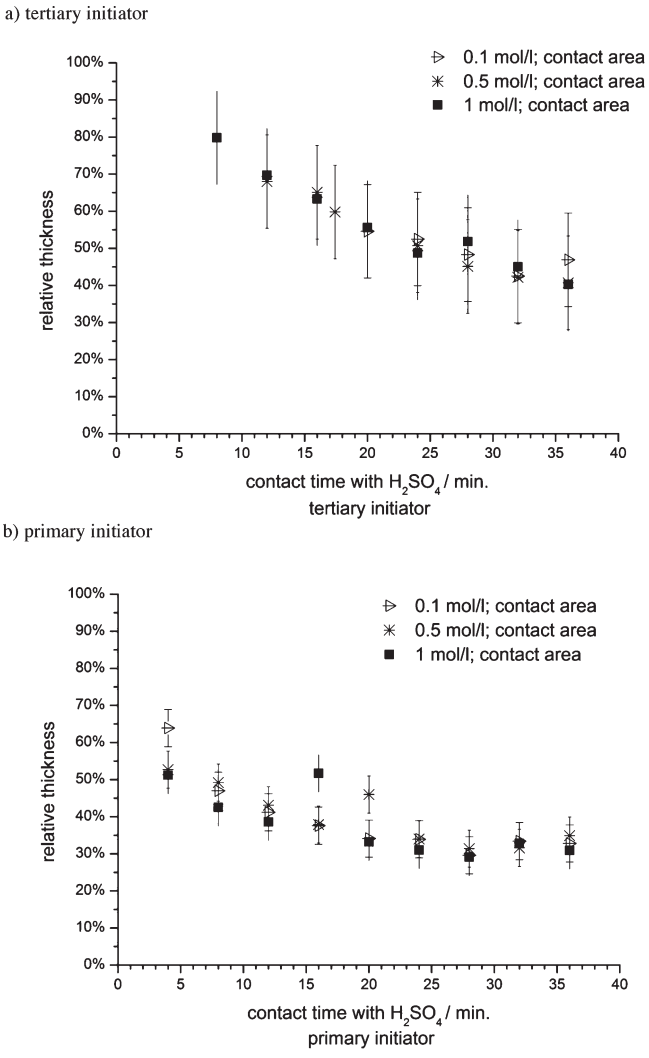

Figure 6. Time dependence of the saponification reaction from inkjet printing. For each concentration a line of droplets was deposited every 4 min. Error bars with long end-caps belong to the data of the 0.1 mol/L sulfuric acid. Error bars with medium end-caps belong to 0.5 mol/L. Error bars with no end-caps indicate data related to 1 mol/L.

adjusted in such a way that the equilibrium is located on the side of the product. In our case the product is the alcohol on the surface and the free bromoisobutyric acid (see Figure 2). The parameters determining the position of the equilibrium are the type of acid used and the amount of water available. With the use of the inkjet printer we were able to screen these parameters simultaneously. In a first attempt we compared two different types of acid, concentrated HCl, and four concentrations of H_2SO_4 (Figure 3). Direct techniques to measure the density of active initiator molecules in an area as small as 60 μm were not available. We therefore measured the film thickness and related this data to changes in grafting density. The more cleaved ester bonds were generated with the acid, the less molecules remained on the surface that still carried bromo functionalities. In turn, this means a reduction in grafting density, resulting in a lower film thickness for a given molecular weight.

We will begin with a discussion of the effect of the various acids on the tertiary initiator (Figure 3a). After treatment with any of the four concentrations of H_2SO_4, no polymer is found within the margin of error ($> 1.2 \pm 1$ nm in every case). In contrast, the film thickness after treatment with concentrated HCl is still 13 nm, which is ~55% of the reference thickness.

Similar observations concerning the effect of concentrated HCl can be made in the case of the primary initiator (Figure 3b). Film thickness after treatment with concentratd HCl is only reduced to 30 nm (75%), whereas on the other hand 6, 3, and 1 mol/L H_2SO_4 reduce the film thickness to 9 nm. This corresponds to 25% of the reference film thickness. 10 mol/L H_2SO_4 shows a significant discrepancy compared to the other H_2SO_4 concentrations. In this case the film thickness was only reduced to 45% (16 nm).

Our motivation for the synthesis of the tertiary initiator was the hydrolytically more labile ester bond in this molecule, which should be easier to cleave. Indeed, for all concentrations of H_2SO_4 and for the HCl, the comparison of relative film thickness of the two initiators show a decrease in relative thickness by 20% or even up to 40% for the 10 mol/L H_2SO_4 in the case of the tertiary initiator. This demonstrates the increased lability of the ester bond in the tertiary initiator. The tertiary initiator combined with diluted H_2SO_4 of 6, 3, or 1 mol/L concentration suppresses polymer growth completely within the margin of error. Yet the primary initiator is interesting to use, when tuning of grafting density is desired.

An explanation for the difference between concentrated HCl and all of the chosen H_2SO_4 is the high volatility of concentrated HCl. HCl has a boiling point of 45 °C[58] (38%), unlike concentrated sulfuric acid, which is nonvolatile with a boiling point of 300−320 °C[59] (96%). The high surface-to-volume ratio of inkjet-printed microdroplets leads to extremely rapid evaporation, even for liquids with boiling points of 200 °C (vapor pressure around 10^{-1} mmHg). Microdroplets of liquids with high boiling point around 200 °C evaporate within ~1 min.[43] Our more quantitative observations are consistent with this argument of volatility. Immediately after deposition the drops of Milli-Q water or concentrated HCl were evaporated. This behavior of HCl is expected, since it is a gas dissolved in water. By contrast, the drops of diluted H_2SO_4 were still present after 20 min, although they seemed to shrink to some extent after deposition due to the loss of water. Video clips of evaporating droplets can be found in the Supporting Information.

Comparison of Effectiveness of Different Concentrations of Sulfuric Acid in Saponification. Next we studied in more detail why 10 mol/L H_2SO_4 was not as effective as lower concentrations, at least in the case of the primary initiator. Our hypothesis is that the water content is solely responsible for the position of the equilibrium of the saponification reaction.

Regardless of the concentration of H_2SO_4 plotted, on the tertiary initiator the remaining film thickness is below 5% of the original thickness (Figure 4a). With all concentrations of 10 to 1 mol/L of H_2SO_4 and a contact time of 20 min, brush growth from the tertiary initiator can be suppressed within the margin of error. For the primary initiator (Figure 4b) the trend to lower thickness with lower concentration of deployed H_2SO_4 is clear-cut. In none of the used concentrations does the thickness go below 20%. So the comparison of the relative film thickness in the contact area between the two initiators for all the different concentrations of H_2SO_4 supports the conclusion that we have drawn from Figure 3. The ester bond is more labile in the tertiary initiator. This effect is independently observed from the value of absolute film thickness, as a comparison of Figures 3 and 4 shows.

The data for both initiators is congruent regarding the effectiveness in saponification of 10 mol/L H_2SO_4. It is lower than all of the more dilute concentrations. This effect is more pronounced for the primary initiator but is in principle also observed for the tertiary initiator. The equilibrium in the

saponification reaction (Figure 2) can be shifted solely by supplying water; protons are just needed as a catalyst. With higher water content, the equilibrium is shifted more and more to the desired side of the alcohol on the surface and the free bromoisobutyric acid. For the tertiary initiator the water content does not seem to be as crucial. This is due to the fact that the ester bond is more labile and breaks easier from the start.

The compliance between the reference thickness (gray) and the nearby (red) again indicates that the droplets did not splash upon contact with the surface (Figure 4).

Polymerized Patterned Surface. After finding the optimum conditions for suppressing polymer growth completely, we wanted to test the potential of our method for printing more complex designs. Since imaging a pattern of several hundred micrometers in size was not possible with the use of the imaging ellipsometer, we printed a pattern with 1 mm in size. With the use of an optical microscope we were able to image this pattern. In Figure 5 the pattern is shown on the right side. It resembles the logo of our institute, which is shown on the left. The pattern was formed by printing 1 mol/L sulfuric acid on the tertiary starter. The film thickness is 8 ± 1 nm as measured by ellipsometry. Polymerization did not occur in the regions where sulfuric acid had been printed. In these regions the film thickness is $>1.2 \pm 1$ nm. The former contact areas appear lighter in the optical microscope image because we measured under moist conditions. The moisture generated a contact angle contrast between the more hydrophobic regions where polymer was grown and the more hydrophilic regions where the initiator was destroyed.

Time Dependence of Saponification Reaction from Inkjet Printing. It would be much more convenient to tune the grafting density by controlling the contact time between the acid and ATRP initiator. Hence, we investigated the time dependence of the saponification reaction. 1 mol/L H_2SO_4 in contact with the surface leads to almost complete defunctionalization of the tertiary initiator. To limit water evaporation, we chose to slow the reaction by cooling the samples to 10 °C and to include lower acid concentrations of 0.5 and 0.1 mol/L H_2SO_4.

The data in Figure 6 are plotted as relative thickness against contact time. We measured the film thickness in four contact areas, plotted the mean value of those, and chose the error of the modeling as error bars (±1 nm).

In Figure 6a there is a gradual decrease in relative brush thickness with contact time for the tertiary initiator. The same holds true in the case of the primary initiator in Figure 6b, but the curve levels off after 20 min within the margin of error. In addition, the data for both initiators show no difference regarding the three concentrations. Given that the water content matters, and not the amount of protons, any concentration below 10 mol/L H_2SO_4 has enough water to shift the equilibrium of the saponification to the product side before the water is evaporated.

When comparing the final thickness for 1 mol/L H_2SO_4 from Figure 4 to Figure 6 for both initiators it is clear that they do not reach the same level, even though the contact time was twice as long. We have altered the sample preparation in the case of the time dependency by cooling the samples to 10 °C. Cooling of the samples slows down the evaporation of water out of the microdroplets, while heating enhances evaporation.[41] This supports our hypothesis that the initial water content of the microdroplet matters. That was the reason why the film thickness decreased with decreasing concentration of H_2SO_4. Then the evaporation of water from the microdroplet set in, and the concentration of H_2SO_4 started to increase. This seems to drive the saponification reaction to completion. Because of the cooling of the substrate, we changed the evaporation of the water from the microdroplet. As a result, a lower fraction of ester molecules was cleaved on the time scale under investigation.

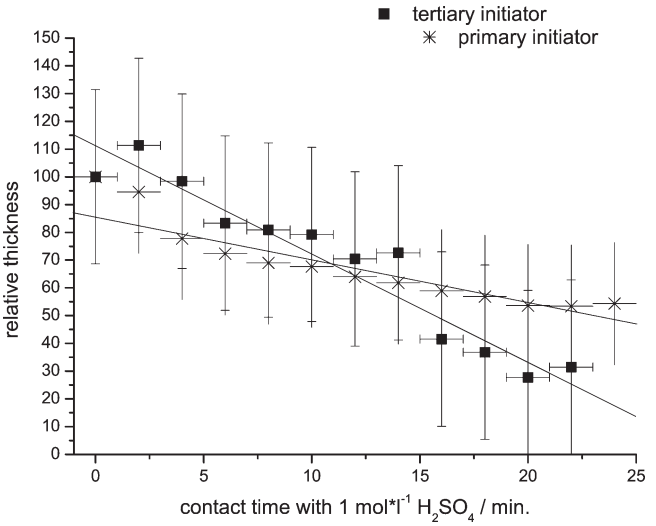

Figure 7. Time dependence of the saponification reaction from dip-coating. The wafers were pulled out of a solution of 1 mol/L H_2SO_4 with a speed of 1.5 mm/min using a dip-coater. Solid lines are guides to the eye. Error bars of the primary starter have no end-caps.

Time Dependence from Dip-Coating/Creation of a Gradient in Grafting Density over the Area of a Whole Wafer. To study the efficiency of the saponification reaction independent of droplet evaporation, we used a dip-coater and gradually pulled out samples from a solution of 1 mol/L H_2SO_4. This approach allowed us to tune the grafting density from brush regime to mushroom regime over larger areas, which is desirable when studying the dependence of brush height on grafting density.[60]

The data in Figure 7 are plotted as relative thickness against contact time. As the point of reference we elected for each initiator (100% relative thickness) the 3 mm wide area that had not been immersed in the H_2SO_4. Measurements of the film thickness were taken at four different areas; we plotted the mean value of this and chose the error of the modeling as error bars (±1 nm).

With longer contact time the grafting density was reduced for both initiators. In analogy to the data in Figure 6 the film thickness in the case of the primary initiator reaches a steady state after 20 min. No steady state is reached for the tertiary initiator, at least not within the contact times under investigation. As is noticeable, the film thickness can be tuned all the way down to 55% for the primary initiator and 30% for the tertiary initiator. Compared to the data from inkjet printing of 1 mol/L H_2SO_4 where we reached levels of 25% for the primary initiator and 5% for the tertiary initiator, the values here are much higher. When using the dip-coater and 20 mL of acid, evaporation plays no role. Thus, the reaction proceeds in a different way, and therefore the saponification reaction did not reach the same conversion as in printing.

AFM Images To Investigate the Effect of the Acid on Areas Surrounding the Droplets. After testing the effect of acid on the SI-ATRP initiators our last step was to study in detail the "ink behavior" on the substrate. A crucial step in ink-printing is the moment a droplet hits the solid substrate and comes to rest. Thus, we turned to AFM to check the features that we created for uniformity and roughness. The AFM images in Figure 8 were taken on the rim of the former

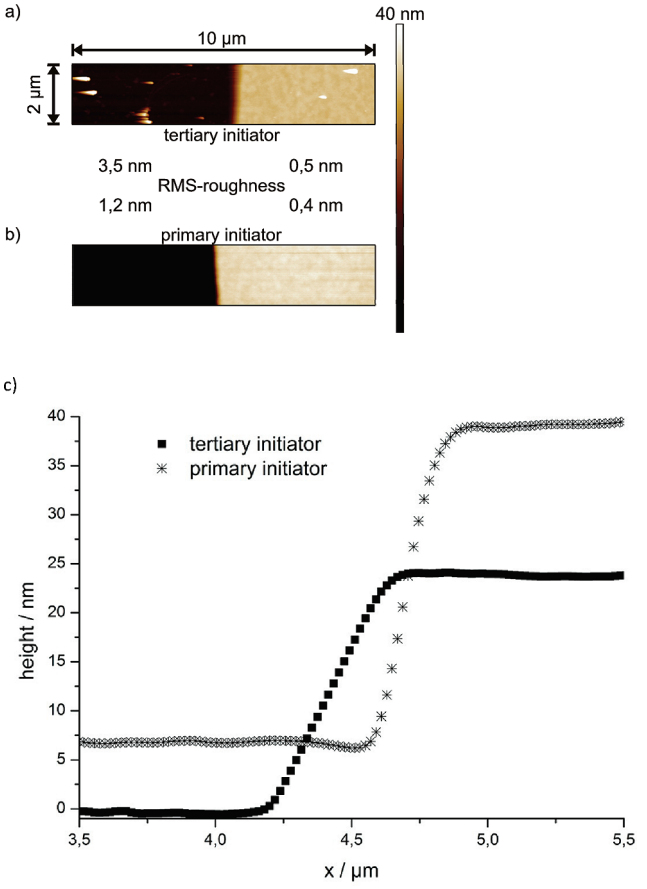

Figure 8. AFM height images taken on the rim of the contact area after the polymerization. Cross sections indicate the structure and the height of the rim.

contact area between 1 mol/L H_2SO_4 and (a) the tertiary initiator and (b) the primary initiator. In both images a sharp step is clearly distinguishable. The step separates the former contact between initiator molecules and the acid from the surrounding PMMA brushes. The cross sections in (c) substantiate this. They clearly show a difference in slope between the two initiators. Within 0.6 μm the transition from the former contact area to unaffected areas is complete in the case of the tertiary initiator. The transition for the primary initiator is completed within 0.4 μm. In the transition areas the change in film thickness is a result of the change in the grafting density of brushes. The difference in slope that we have observed has its origin in the combination of droplet evaporation and ester bond lability. For the tertiary starter the evaporation sets in while the saponification proceeds and the droplet shrinks in size. In the case of the primary starter saponification is slower, and therefore the greater part of the saponification takes place after the shrinking of the droplet has proceeded.

The heights of the rim indicated in the cross sections from AFM (Figure 8c) are now compared to the ellipsometry data. Given that AFM can only measure relative height differences, we chose the reference thickness from ellipsometry measurement as the highest point of the cross section.

For the tertiary initiator (filled squares) AFM gave a height of the rim of 24 nm, which is in good comparison to 23 $\pm$ 1 nm calculated from ellipsometry data. In the case of the primary initiator (stars) ellipsometry yielded a height of 31 $\pm$ 1 nm compared to 33 nm from AFM.

Concerning the rms roughness of the surrounding PMMA layers, we obtained 0.5 nm for the tertiary initiator and 0.4 nm for the primary one. Ramakrishnan et al.[54] published a roughness of 0.5 nm for the PMMA layer from X-ray reflectivity measurements in the case of the primary initiator. The agreement between the roughness of the PMMA brushes around the pattern between the two tested ATRP initiators and the roughness from the literature demonstrates that the acid did not have any effect on the surrounding areas and in turn catalyzed the saponification reaction only in the printed areas.

Conclusions and Outlook

We have demonstrated that chemistry with an inkjet printer is feasible. The industrial relevance of inkjet printing is related to the potential for automation and high throughput. In our case the inkjet printer was used to deposit microdroplets of acid. Within these microdroplets we carried out the saponification of surface-immobilized ATRP initiators containing an ester bond. The changes in the monolayer of ester molecules due to saponification were amplified by SI-ATRP. The polymer brush thickness was then related to effectiveness of saponification. The use of an inkjet printer allowed us to screen parameters such as type of acid, concentration of acid, and contact time between acid and surface simultaneously. Additionally, we utilized a dip-coater to test the saponification independent of droplet evaporation.

The advantage of the developed process is that it is applicable to all surface-immobilized initiators containing ester bonds.

In future research we plan to use our process to defunctionalize the initiator molecules covering a microcantilever. If we do this selectively on one side of a cantilever, we can generate an asymmetric coating of the cantilever with polymer brushes. An asymmetric coating allows the use of a microcantilever for sensing applications.[49]

Acknowledgment. S. G. J. Emmerling (GU 771/3) and S. A. Pihan (BE 3286/1) gratefully acknowledge financial support of the Deutsche Forschungsgemeinschaft (DFG) under the SPP1369 Priority Program (Polymer-Solid Contacts: Interfaces and Interphases). P. Lellig (GU 771/2) gratefully acknowledges the DFG-SPP1181 for financial support. Special thanks are given to Gunnar Kircher, Sebastian Nett, and E. Bryan Coughlin for helpful discussions.

Supporting Information Available: Correction of optical distortion along the beam explaining the calculation of feature size on the sample, correlation of film thickness with M_n of polymer grown in solution showing the control of the polymerization process, tables with molecular weight and polydispersity of polymer grown in solution, tables with grafting density of polymer brushes, video clips demonstrating the evaporation of single droplets of HCl and H_2SO_4. This material is available free of charge via the Internet at http://pubs.acs.org.

References and Notes

(1) Schmelmer, U.; Jordan, R.; Geyer, W.; Eck, W.; Golzhauser, A.; Grunze, M.; Ulman, A. *Angew. Chem., Int. Ed.* **2003**, *42* (5), 559.
(2) Farhan, T.; Huck, W. T. S. *Eur. Polym. J.* **2004**, *40* (8), 1599–1604.
(3) Li, H. W.; Muir, B. V. O.; Fichet, G.; Huck, W. T. S. *Langmuir* **2003**, *19* (6), 1963–1965.
(4) Advincula, R. C.; Brittain, W. J.; Baster, K. C.; Rühe, J. *Polymer Brushes: Synthesis, Characterization, Applications*; Wiley-VCH: Weinheim, 2004.
(5) Prucker, O.; Rühe, J. *Macromolecules* **1998**, *31* (3), 592–601.
(6) Zhao, B.; Brittain, W. J. *Prog. Polym. Sci.* **2000**, *25* (5), 677–710.
(7) Husseman, M.; Malmstrom, E. E.; McNamara, M.; Mate, M.; Mecerreyes, D.; Benoit, D. G.; Hedrick, J. L.; Mansky, P.; Huang, E.; Russell, T. P.; Hawker, C. J. *Macromolecules* **1999**, *32* (5), 1424–1431.
(8) Baum, M.; Brittain, W. J. *Macromolecules* **2002**, *35*, 610–615.

(9) Barner-Kowollik, C. *Handbook of RAFT*; Wiley-VCH: Weinheim, Germany, 2008.
(10) Matyjaszewski, K.; Xia, J. *Chem. Rev.* **2001**, *101*, 2921–2990.
(11) Pyun, J.; Kowalewski, T.; Matyjaszewski, K. *Macromol. Rapid Commun.* **2003**, *24* (18), 1043–1059.
(12) Boyes, S. G.; Granville, A. M.; Baum, M.; Akgun, B.; Mirous, B. K.; Brittain, W. J. *Surf. Sci.* **2004**, *570* (1−2), 1–12.
(13) Matyjaszewski, K.; Miller, P. J.; Shukla, N.; Immaraporn, B.; Gelman, A.; Luokala, B. B.; Siclovan, T. M.; Kickelbick, G.; Vallant, T.; Hoffmann, H.; Pakula, T. *Macromolecules* **1999**, *32* (26), 8716–8724.
(14) Kong, X. X.; Kawai, T.; Abe, J.; Iyoda, T. *Macromolecules* **2001**, *34* (6), 1837–1844.
(15) von Werne, T.; Patten, T. E. *J. Am. Chem. Soc.* **1999**, *121* (32), 7409–7410.
(16) von Werne, T.; Patten, T. E. *J. Am. Chem. Soc.* **2001**, *123* (31), 7497–7505.
(17) Carlmark, A.; Malmstrom, E. *J. Am. Chem. Soc.* **2002**, *124* (6), 900–901.
(18) Zhao, H. Y.; Farrell, B. P.; Shipp, D. A. *Polymer* **2004**, *45* (13), 4473–4481.
(19) Edmondson, S.; Osborne, V. L.; Huck, W. T. S. *Chem. Soc. Rev.* **2004**, *33* (1), 14–22.
(20) Tovar, G.; Paul, S.; Knoll, W.; Prucker, O.; Rühe, J. *Supramol. Sci.* **1995**, *2* (2), 89–98.
(21) Rühe, J. In *Polymers Grafted from Solid Surfaces*, 6th Dresden Polymer Discussion on Surface Modification, Meissen, Germany, Apr 14−17; Jacobasch, H. J., Ed.; Huthig & Wepf Verlag: Meissen, Germany, 1997; pp 215−222.
(22) Tsai, I. Y.; Crosby, A. J.; Russell, T. P. Surface patterning. In *Cell Mechanics*; Academic Press: San Diego, 2007; Vol. *83*, pp 67−87.
(23) Husemann, M.; Morrison, M.; Benoit, D.; Frommer, K. J.; Mate, C. M.; Hinsberg, W. D.; Hedrick, J. L.; Hawker, C. J. *J. Am. Chem. Soc.* **2000**, *122* (8), 1844–1845.
(24) Ducker, R.; Garcia, A.; Zhang, J. M.; Chen, T.; Zauscher, S. *Soft Matter* **2008**, *4* (9), 1774–1786.
(25) Kaholek, M.; Lee, W. K.; LaMattina, B.; Caster, K. C.; Zauscher, S. *Nano Lett.* **2004**, *4* (2), 373–376.
(26) Zapotoczny, S.; Benetti, E. M.; Vancso, G. J. *J. Mater. Chem.* **2007**, *17* (31), 3293–3296.
(27) Kumar, A.; Whitesides, G. M. *Appl. Phys. Lett.* **1993**, *63* (14), 2002–2004.
(28) Xia, Y. N.; Whitesides, G. M. *Angew. Chem., Int. Ed.* **1998**, *37* (5), 551–575.
(29) Husemann, M.; Mecerreyes, D.; Hawker, C. J.; Hedrick, J. L.; Shah, R.; Abbott, N. L. *Angew. Chem., Int. Ed.* **1999**, *38* (5), 647–649.
(30) Shah, R. R.; Merreceyes, D.; Husemann, M.; Rees, I.; Abbott, N. L.; Hawker, C. J.; Hedrick, J. L. *Macromolecules* **2000**, *33* (2), 597–605.
(31) Jones, D. M.; Huck, W. T. S. *Adv. Mater.* **2001**, *13* (16), 1256–1259.
(32) Jones, D. M.; Smith, J. R.; Huck, W. T. S.; Alexander, C. *Adv. Mater.* **2002**, *14* (16), 1130–1134.
(33) Zhou, F.; Huck, W. T. S. *Chem. Commun.* **2005**, *48*, 5999–6001.
(34) Zhou, F.; Zheng, Z. J.; Yu, B.; Liu, W. M.; Huck, W. T. S. *J. Am. Chem. Soc.* **2006**, *128* (50), 16253–16258.
(35) Love, J. C.; Wolfe, D. B.; Chabinyc, M. L.; Paul, K. E.; Whitesides, G. M. *J. Am. Chem. Soc.* **2002**, *124* (8), 1576–1577.
(36) Dyer, D. J. *Adv. Funct. Mater.* **2003**, *13* (9), 667–670.
(37) Jeon, N. L.; Choi, I. S.; Whitesides, G. M.; Kim, N. Y.; Laibinis, P. E.; Harada, Y.; Finnie, K. R.; Girolami, G. S.; Nuzzo, R. G. *Appl. Phys. Lett.* **1999**, *75* (26), 4201–4203.
(38) Kim, N. Y.; Jeon, N. L.; Choi, I. S.; Takami, S.; Harada, Y.; Finnie, K. R.; Girolami, G. S.; Nuzzo, R. G.; Whitesides, G. M.; Laibinis, P. E. *Macromolecules* **2000**, *33* (8), 2793–2795.
(39) Tu, H.; Heitzman, C. E.; Braun, P. V. *Langmuir* **2004**, *20* (19), 8313–8320.
(40) Calvert, P. *Chem. Mater.* **2001**, *13* (10), 3299–3305.
(41) Tekin, E.; Smith, P. J.; Schubert, U. S. *Soft Matter* **2008**, *4* (4), 703–713.
(42) Derby, B.; Reis, N. *MRS Bull.* **2003**, *28* (11), 815–818.
(43) Shimoda, T.; Morii, K.; Seki, S.; Kiguchi, H. *MRS Bull.* **2003**, *28* (11), 821–827.
(44) Burns, S. E.; Cain, P.; Mills, J.; Wang, J. Z.; Sirringhaus, H. *MRS Bull.* **2003**, *28* (11), 829–834.
(45) Zaugg, F. G.; Wagner, P. *MRS Bull.* **2003**, *28* (11), 837–842.
(46) Sankhe, A. Y.; Booth, B. D.; Wiker, N. J.; Kilbey, S. M. *Langmuir* **2005**, *21* (12), 5332–5336.
(47) Ramakrishnan, A.; Dhamodharan, R.; Rühe, J. *J. Polym. Sci., Part A: Polym. Chem.* **2006**, *44* (5), 1758–1769.
(48) deGennes, P. G. *Macromolecules* **1980**, *13* (5), 1069–1075.
(49) Bumbu, G. G.; Kircher, G.; Wolkenhauer, M.; Berger, R.; Gutmann, J. S. *Macromol. Chem. Phys.* **2004**, *205* (13), 1713–1720.
(50) Azzam, N. M.; Bashara, R. M. A. *Ellipsometry and Polarized Light*; North-Holland: Amsterdam, 1977.
(51) Sormunen, G. J.; Lewis, D. E. *Synth. Commun.* **2004**, *34* (19), 3473–3480.
(52) Einhorn, A.; Hollandt, F. *Justus Liebigs Ann. Chem.* **1898**, *301* (1), 95–115.
(53) Marciniec, B.; Gulinski, J.; Urbaniak, W.; Kornetka, Z. W. *Comprehensive Handbook on Hydrosilylation*; Pergamon Press: Elmsford, NY, 1993.
(54) Ramakrishnan, A.; Dhamodharan, R.; Rühe, J. *Macromol. Rapid Commun.* **2002**, *23*, 612–616.
(55) Kawase, T.; Shimoda, T.; Newsome, C.; Sirringhaus, H.; Friend, R. H. In *Inkjet Printing of Polymer Thin Film Transistors*, 5th International Conference on Nano-Molecular Electronics (ICNME2002), Kobe, Japan, Dec 10−12; Elsevier Science: Kobe, Japan, 2002; pp 279−287.
(56) Nett, S. K.; Kircher, G.; Gutmann, J. S. *Macromol. Chem. Phys.* **2009**, *210* (11), 971–976.
(57) Miyake, T.; Tanii, T.; Kato, K.; Hosaka, T.; Kanari, Y.; Sonobe, H.; Ohdomari, I. *Chem. Phys. Lett.* **2006**, *426* (4−6), 361–364.
(58) Hydrochloric acid - boiling point. http://www.solvaychlorinatedinorganics.com/docroot/chlo_inorg/static_files/attachments/pch_1300_0005_w_en_ww.pdf.
(59) Sulfuric acid. http://www.inorganics.basf.com/p02/CAPortal/en_GB/portal/Anorganische_Basen_/content/Produktgruppen/Anorganische_Basen_(Laugen)/Produktinformationen/Schwefelsaeure.
(60) Wu, T.; Efimenko, K.; Genzer, J. *J. Am. Chem. Soc.* **2002**, *124* (32), 9394–9395.